中国激光

铝/镀镍钢异种材料摆动激光熔钎焊接头组织性能

刘永洪，蔡创*，谢佳，张冰冰，余杰，黄嘉森

西南交通大学材料科学与工程学院材料先进技术教育部重点实验室，四川 成都 610031

摘要 界面金属间化合物的厚度和种类是影响铝/钢异种材料激光熔钎焊接头性能的关键。研究了不同摆动参数下接头金属间化合物(IMCs)的厚度和种类，并进一步分析了不同摆动参数下接头的拉伸性能及断口形貌。结果表明，摆动激光可以改善铝/钢异种材料激光熔钎焊接头界面金属间化合物的厚度和相组成。未加摆动激光时，在界面形成了厚度约为8.45 μm的两层IMCs，焊缝侧IMCs为τ_5-(Fe，Ni)$_{1.8}$Al$_{7.2}$Si，钢侧IMCs为θ-(Fe，Ni)(Al，Si)$_3$。当激光摆动直径为2 mm、频率为30 Hz时，IMCs的分布更加连续均匀，厚度约为2.21 μm，界面层组织为τ_5-(Fe，Ni)$_{1.8}$Al$_{7.2}$Si，最优接头线载荷为289.1 N/mm，比未加摆动激光时的接头线载荷提高了约33.9%。

关键词 激光技术；铝/钢激光熔钎焊；摆动激光；金属间化合物；力学性能

中图分类号 TG457.1 **文献标志码** A **DOI**: 10.3788/CJL231051

1 引 言

轻量化是汽车、地铁以及航空等领域关键结构的主要发展趋势。在工业快速发展和节能减排的大环境下，行业对材料性能的要求越来越高。采用低密度的轻质材料如铝合金等代替传统的钢、钛等材料制备异种材料复合结构是实现轻量化的重要手段之一[1-3]。

由于铝合金和钢的物理和化学性质不同，采用熔焊技术将铝与钢连接起来往往难以实现，且铁元素和铝元素之间的固溶度小，易在界面层产生脆性金属间化合物(IMCs)[4]。铝合金和钢的焊接接头的断裂行为与IMCs层的形态和厚度有关，因为性能差且临界应力强度低的金属间化合物有利于裂纹扩展[5-6]。且抗拉强度会随着IMCs层厚度的增加而降低[7-8]，因为微裂纹通常始于IMCs相对较厚的位置[9]。Xia等[10]通过原位扫描电镜(SEM)发现，相比界面层中有较厚的$\tau_5+\theta$或$\tau_5+\theta+\eta$相，当界面层中只有较薄的τ_5-Fe$_{1.8}$Al$_{7.2}$Si相时，抗拉强度较高，因为τ_5-Fe$_{1.8}$Al$_{7.2}$Si相会阻碍裂纹沿钢和τ_5-Fe$_{1.8}$Al$_{7.2}$Si相之间的界面扩展。

目前，国内外学者进行异种材料焊接时，通常采用优化热输入、超声波辅助、调整焊接工艺、添加中间层、添加填充焊丝等来改善界面金属间化合物层[11-12]。有学者发现，IMCs层的厚度随着热输入的增加而增加[13-15]。而摆动激光可改善激光的能量分布，降低峰值能量[16]。Xie等[17]在加入摆动激光后发现，界面峰值温度降低，抑制了金属间化合物的形成，降低了金属间化合物层的厚度。Jiang等[18]发现，横向激光振荡使焊缝中心附近的金属液温度分布更加均匀，甚至出现负温度梯度。杨晖等[19]发现，接头在摆动频率较高、摆动幅度较大的情况下会出现咬边缺陷。Chen等[20-22]采用激光熔钎焊结合冷金属转移(CMT)电弧工艺和双激光束激光熔钎焊工艺，通过控制激光束向Al侧偏移，获得了成形良好的接头，促进了界面间金属化合物的均匀分布。Tan等[23]研究了不同镍镀层厚度对显微组织和力学性能的影响，发现随着涂层厚度的增加，金属间化合物层的厚度增加，断裂载荷先增大后减小。Chen等[24-25]发现界面层的形态与温度有关。Yang等[26-27]通过添加镀镍层抑制脆性相的形成，提升了接头的力学性能。但同时Ni与Si之间易反应生成Ni_2Si[28-30]，所以应尽量控制镀镍层的厚度。董斌鑫等[31]通过调整保护气中的氧含量来调控异种材料的焊接质量。Yang等[32]使用锌铝合金(Zn-22Al)作为填充金属，在铝/钢接头的界面金属间化合物基体中出现弥散现象，提升了接头强度。Yu等[33]发现，含有Si元素的焊丝不仅可以提高激光熔钎焊过程中焊接接头的润湿铺展性，也能降低IMCs层的厚度。

本文采用镀镍层优化界面反应，通过摆动激光改善温度分布及优化界面反应，实现铝/钢异种材料的优质连接。分析了不同激光摆动参数下铝/钢激光熔钎焊接头界面层形貌、种类和厚度的变化，对铝/钢焊接接头的力学性能进行了研究，并进一步研究了接头的

收稿日期：2023-07-24；**修回日期**：2023-08-17；**录用日期**：2023-09-11；**网络首发日期**：2023-09-22

基金项目：国家自然科学基金(52375386，51805456)、先进焊接与连接国家重点实验室开放课题研究基金(AWJ-23M18)

通信作者：*caichuang@home.swjtu.edu.cn

断口形貌和断裂模式。

2 试验材料及方法

2.1 试验材料

试验材料是尺寸为100.0 mm×80.0 mm×0.9 mm的304不锈钢板与尺寸为100.0 mm×80.0 mm×1.2 mm的6061-T6铝合金板材，所用焊丝为直径为1.6 mm的AlSi12焊丝。试验材料和焊丝的化学成分如表1所示。为了提高焊接过程中焊丝的润湿性和铺展性，抑制铝/钢界面脆性金属间化合物的生成，并降低金属间化合物层的厚度，试验开始前在不锈钢板表面进行镀镍，在电流密度为1 A/dm^{2}的镍溶液中电镀30 min。镀镍溶液由157.6 mL水、20.2 g $NiCl_2$•$6H_2O$、81.2 g $NiSO_4$•$6H_2O$和8.0 g H_3BO_3组成。钢表面上的镍涂层如图1所示。焊前对铝合金进行机械打磨，去氧化层，用乙醇擦拭镀镍钢。

表1 6061-T6铝合金、304不锈钢板和AlSi12焊丝的化学成分

Table 1 Chemical compositions of 6061-T6 aluminum alloy, 304 stainless steel, and AlSi12 filler wire

Material	Mass fraction /%												
	Si	Fe	Cu	Mg	Mn	Cr	Ti	Al	C	P	Ni	Mo	Zn
6061-T6	0.644	0.297	0.263	0.944	0.037	0.168	0.033	Bal.	–	–	–	–	–
304	0.584	Bal.	–	–	1.103	17.970	–	–	0.031	0.030	8.218	0.039	–
AlSi12	12.00	0.80	0.30	0.10	0.15	–	0.15	Bal.	–	–	–	–	0.20

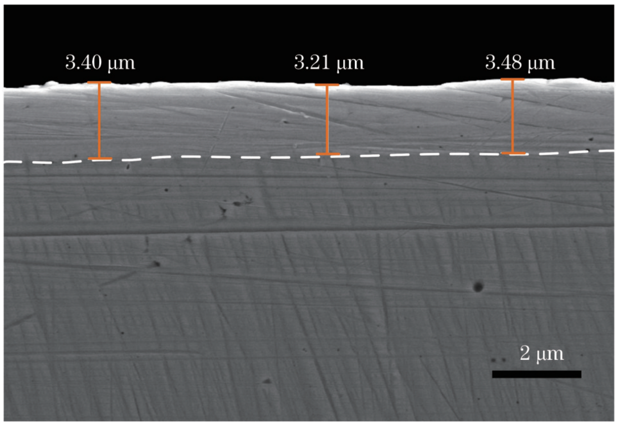

图1 钢表面的镀镍层

Fig. 1 Ni coating layer on surface of steel

2.2 试验设备及方法

焊接采用4 kW光纤激光器，波长为1060 nm，焦距为250 mm。焊丝与水平面的夹角为30°，激光束与竖直方向的夹角为10°，激光光斑和焊丝端部之间的距离为0 mm，试验装置如图2所示。为了使焊丝和铝合金充分熔化并在不锈钢表面润湿铺展，进而填充到铝/钢搭接接头的间隙中形成熔钎焊焊缝，达到良好焊接效果，设置激光束的离焦量为+30 mm。采用气流量为25 L/min的高纯氩(体积分数为99.99%)作为保护气。焊接过程中激光功率、焊接速度和送丝速度为常值，激光摆动方式为圆形摆动。其他参数如表2所示，其中P为激光功率，V_h为焊接速度，V_s为送丝速度，d为摆动直径，f为摆动频率。

2.3 组织分析和力学性能测试

焊接后制备尺寸为20 mm×10 mm的焊缝金相试样。通过金相显微镜观察焊缝的横截面形貌。扫描电子显微镜(SEM)配备的背散射电子探测器用于分析IMCs层的形貌和厚度。采用配备在SEM仪器上的能

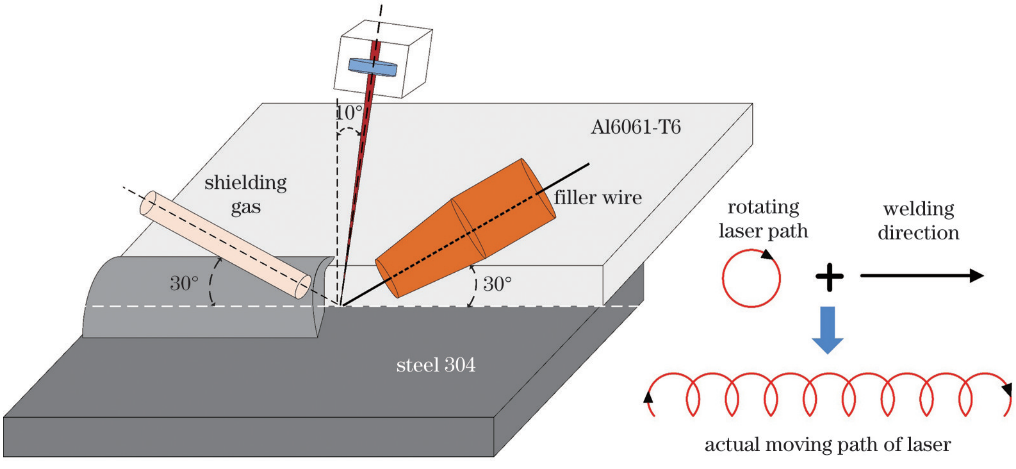

图2 摆动激光熔钎焊装置示意图

Fig. 2 Schematic of rotating laser welding-brazing device

表 2 摆动激光熔钎焊工艺参数

Table 2 Process parameters of rotating laser welding-brazing

No.	P /W	V_h /(mm/s)	V_s /(mm/s)	d /mm	f /Hz
1	2800	10	33	0	0
2	2800	10	33	1	30
3	2800	10	33	2	30
4	2800	10	33	3	30
5	2800	10	33	4	30
6	2800	10	33	2	10
7	2800	10	33	2	50
8	2800	10	33	2	70
9	2800	10	33	2	80

量色散光谱仪(EDS)检测界面层的化学成分。制备三组尺寸为 80 mm×15 mm 的拉伸试样。为了减小界面润湿面积对接头力学性能的影响,接头的力学性能用线载荷(F/W,其中 F 为最大负载,W 为拉伸试样的宽度)表示,单位为 N/mm。通过 SEM 二次电子探测器观察断口形貌。

3 结果与分析

3.1 摆动激光对界面润湿性的影响

图 3 所示为不同摆动直径和不同摆动频率下的接头形貌。摆动激光对润湿宽度的影响如图 4 所示。将摆动直径和频率分别为 0 mm 和 0 Hz(不摆动)的接头作为对照组,如图 3(a)所示。在激光未摆动以及激光摆动直径为 2 mm 的情况下,可以获得均匀的焊缝。在这些情况下,铝合金大量熔化并形成良好的连接,如图 3(a)、(c)所示。当激光摆动直径为 1 mm 时,焊缝金属填充不均匀,接头润湿宽度显著减小,如图 4(a)所示。当摆动直径增加到 3~4 mm 时,激光作用区域中心处的能量密度降低,导致铝合金熔化较少,润湿宽度减小。当摆动频率为 10 Hz 时,激光热源与焊丝重叠率较低,焊丝熔化不良,接头润湿宽度减小,如图 4(b)所示。当摆动频率为 70~80 Hz 时,较高的摆动频率可以提高热源的重叠率,熔融铝合金在钢表面上的铺展能力得到改善。此外,与摆动频率相比,摆动直径对润湿宽度的影响更为显著。为了获得成形良好的激光熔钎焊铝/钢异种接头,应在激光摆动直径为 2 mm 时优化焊接参数。

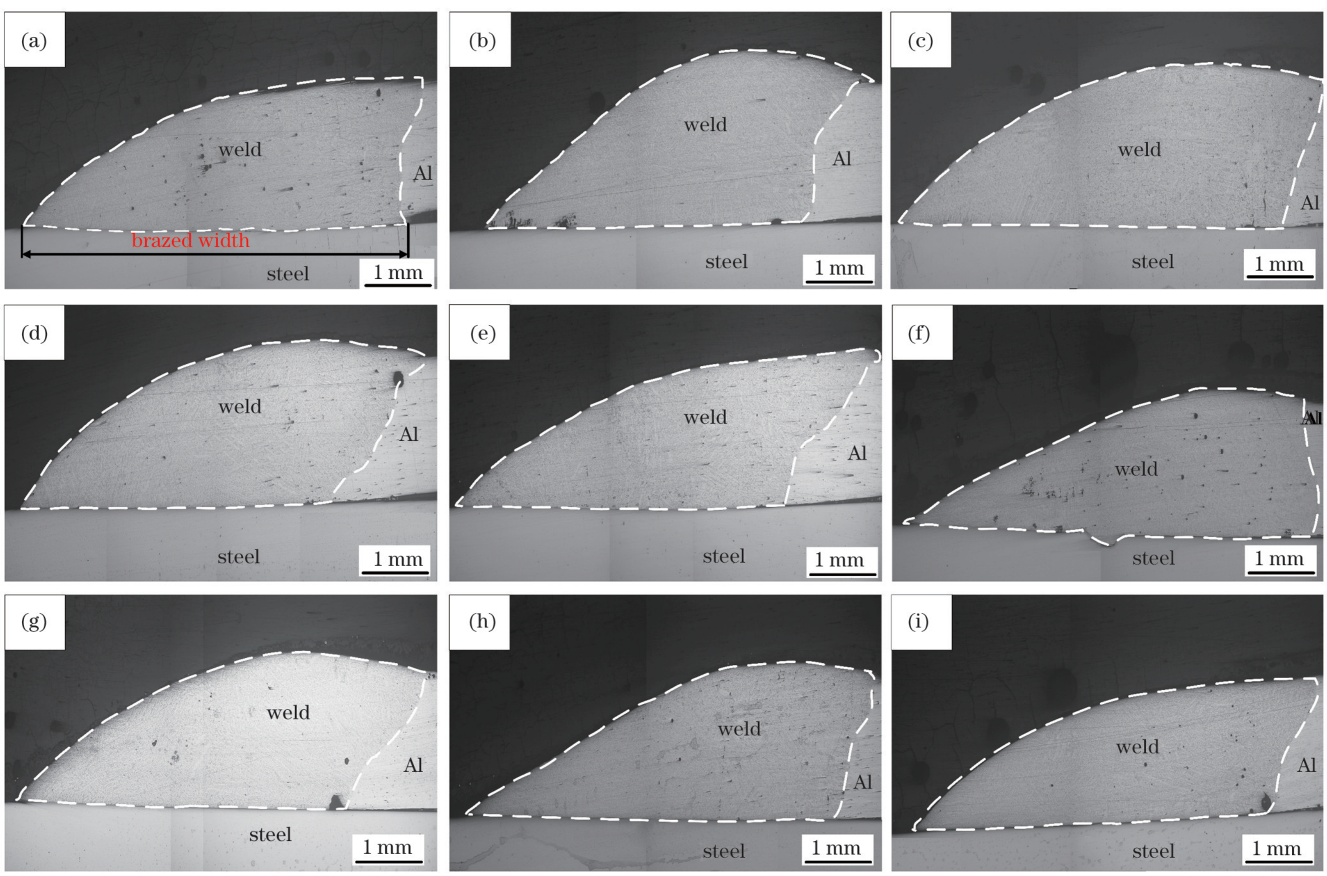

图 3 接头横截面和润湿宽度。(a)无摆动激光模式;摆动直径为(b) 1 mm、(c) 2 mm、(d) 3 mm、(e) 4 mm;摆动频率为(f) 10 Hz、(g) 50 Hz、(h) 70 Hz、(i) 80 Hz

Fig. 3 Joint cross sections and wetting widths. (a) Without rotating laser mode; rotating diameter is (b) 1 mm, (c) 2 mm, (d) 3 mm, (e) 4 mm; rotating frequency is (f) 10 Hz, (g) 50 Hz, (h) 70 Hz, (i) 80 Hz

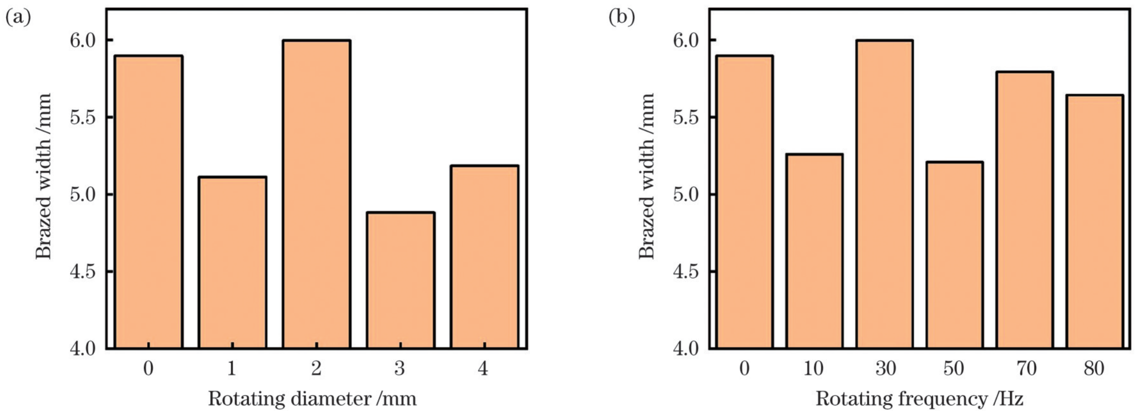

图 4 激光摆动参数对润湿宽度的影响。(a)摆动直径；(b)摆动频率

Fig. 4 Effects of laser rotating parameters on wetting width. (a) Rotating diameter; (b) rotating frequency

3.2 摆动激光对界面层的影响

不同激光摆动直径和频率下焊缝/钢界面区域的SEM图像如图5、6所示，标记区域的EDS分析结果如表3所示。未加摆动激光时，在界面处形成了连续性较差且平均厚度为8.45 μm的两层IMCs，如图5(a)所示。EDS结果显示，焊缝侧IMCs为τ_5-(Fe，Ni)$_{1.8}$Al$_{7.2}$Si，

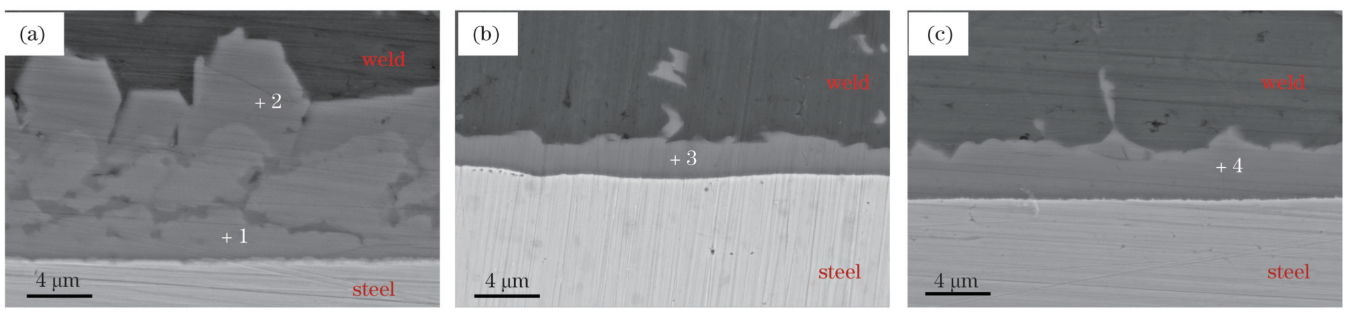

图 5 不同摆动直径下焊缝/钢界面区域的SEM图像。(a) 0 mm；(b) 2 mm；(c) 4 mm

Fig. 5 SEM images of weld /steel interfacial regions under different rotating diameters. (a) 0 mm; (b) 2 mm; (c) 4 mm

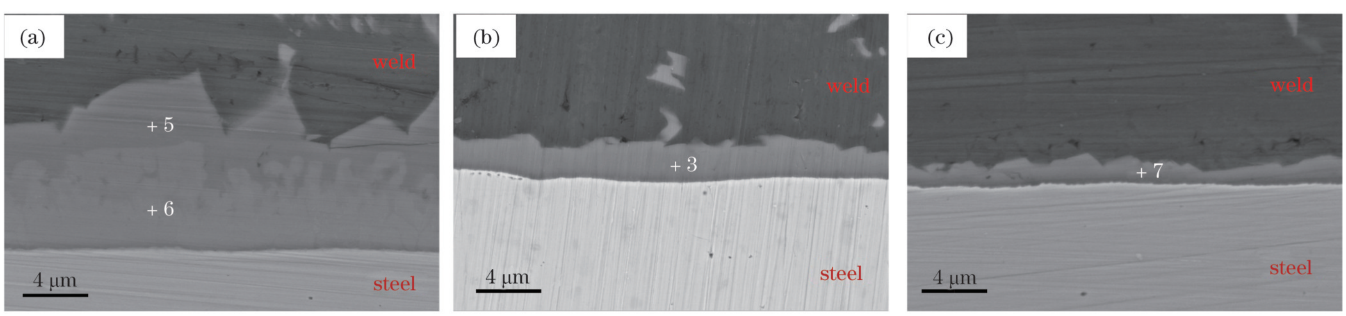

图 6 不同摆动频率下焊缝/钢界面区域的SEM图像。(a) 10 Hz；(b) 30 Hz；(c) 50 Hz

Fig. 6 SEM images of weld/steel interfacial regions under different rotating frequencies. (a) 10 Hz; (b) 30 Hz; (c) 50 Hz

表 3 图5和图6中标记区域的EDS结果

Table 3 EDS results of marked zones in Fig. 5 and Fig. 6

No.	Atomic fraction /%					Possible phase	Thickness /μm
	Al	Si	Fe	Ni	Cr		
1	61.91	8.70	20.67	1.37	7.34	θ-(Fe, Ni)(Al, Si)$_3$	8.45
2	72.19	10.29	12.36	0.16	4.99	τ_5-(Fe, Ni)$_{1.8}$Al$_{7.2}$Si	–
3	72.12	10.58	11.16	1.55	4.59	τ_5-(Fe, Ni)$_{1.8}$Al$_{7.2}$Si	2.21
4	72.08	10.20	12.49	0.55	4.67	τ_5-(Fe, Ni)$_{1.8}$Al$_{7.2}$Si	3.24
5	72.03	8.90	13.44	0.32	5.32	τ_5-(Fe, Ni)$_{1.8}$Al$_{7.2}$Si	–
6	61.78	7.78	21.68	1.50	7.26	θ-(Fe, Ni) (Al, Si)$_3$	6.48
7	71.08	9.94	12.64	0.45	5.89	τ_5-(Fe, Ni)$_{1.8}$Al$_{7.2}$Si	1.53

钢侧IMCs为θ-(Fe,Ni)(Al,Si)$_3$。镍涂层抑制了Fe原子的扩散，并取代Fe原子与Al原子反应，这有利于改善Al原子与Fe原子之间的界面反应，在一定程度上可以抑制脆性金属间化合物层的形成[34-35]。随着摆动直径的变化，IMCs的形态发生较大改变。当摆动直径为2 mm时，在界面处观察到连续均匀的IMCs，平均厚度为2.21 μm，EDS结果显示界面层组织为τ_5-(Fe,Ni)$_{1.8}$Al$_{7.2}$Si。当摆动直径为4 mm时，界面层组织为τ_5-(Fe,Ni)$_{1.8}$Al$_{7.2}$Si，平均厚度为3.24 μm，如图5(c)所示。加入摆动激光后，θ-(Fe,Ni)(Al,Si)$_3$和τ_5-(Fe,Ni)$_{1.8}$Al$_{7.2}$Si组成的IMCs的厚度显著降低，IMCs层均匀性提高。

采用摆动激光熔钎焊后，在界面处形成了致密的IMCs，但当摆动频率在10～50 Hz范围内变化时，界面层形貌有较大差异。随着频率的增加，IMCs厚度明显减小，如图6(a)～(c)所示。当摆动频率为10 Hz时，界面处形成了平均厚度为6.48 μm的两层IMCs，如图6(a)所示，EDS结果如表3所示，焊缝侧的IMCs为τ_5-(Fe,Ni)$_{1.8}$Al$_{7.2}$Si，靠近钢侧的IMCs为θ-(Fe,Ni)(Al,Si)$_3$。当摆动频率为50 Hz时，界面处形成了厚度为1.73 μm的单层IMCs，EDS结果显示界面层组织为τ_5-(Fe,Ni)$_{1.8}$Al$_{7.2}$Si，如图6(c)所示。

3.3 接头的力学性能

采用合适的激光摆动参数可以显著提高铝/钢接头的力学性能。如图7所示，不加摆动激光时接头的线载荷为215.9 N/mm。当摆动直径从1 mm增加到2 mm时，接头线载荷显著增大。摆动直径为2 mm的接头的线载荷最大，为289.1 N/mm，相比于未加摆动时接头线载荷提高了约33.9%，如图7(a)所示。当摆动直径增加到3～4 mm时，接头线载荷较2 mm时减小。当摆动频率为10～50 Hz时，接头线载荷高于不摆动时。在摆动频率为50 Hz的情况下，线载荷为245.8 N/mm，如图7(b)所示。当摆动频率在70～80 Hz范围内时，接头线载荷进一步减小。与未加摆动激光的接头相比，摆动激光熔钎焊接头的线载荷增大，这是由于金属间化合物层的厚度减小，且金属间化合物的种类减少。

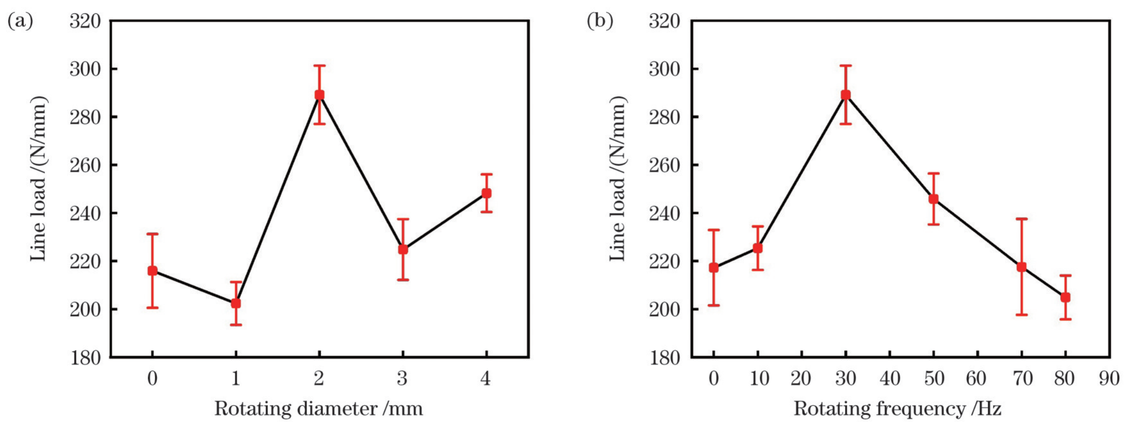

图7 不同摆动参数下接头的线载荷。(a)摆动直径；(b)摆动频率

Fig. 7 Line loads of joints under different rotating parameters. (a) Rotating diameter; (b) rotating frequency

3.4 断裂行为分析

为了阐明铝/钢异种接头的界面显微组织与力学性能之间的关系，研究了接头的断裂行为。分析发现，存在图8所示的两种断裂模式，沿界面层断裂和沿焊缝断裂。摆动直径为1 mm、频率为30 Hz时获得的接头性能最差，在界面处断裂，如图8(a)所示。同样的断裂方式也出现在摆动频率为10、70、80 Hz和摆动直径为0 mm、3 mm时。当摆动直径为2 mm、摆动频率为30 Hz时接头具有最高线载荷，接头断裂在焊缝处。同样的断裂方式也出现在摆动直径为2 mm、摆动频率

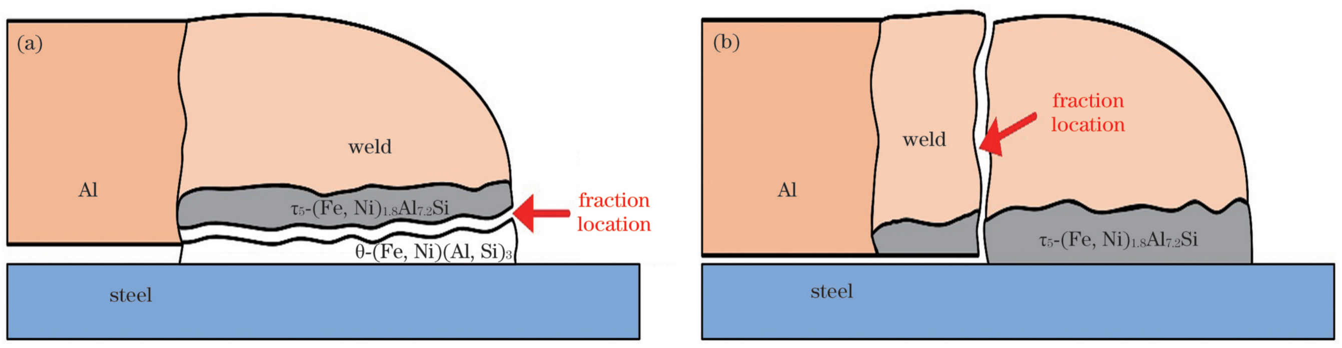

图8 两种断裂模式。(a)断裂在界面处；(b)断裂在焊缝处

Fig. 8 Schematics of two fracture modes. (a) Fracture at interface; (b) fracture at weld

为50 Hz时，线载荷高于在界面处断裂的接头。接头在摆动直径为2 mm、频率为30～50 Hz时表现出良好的力学性能。

接头断裂区域的断口形貌和EDS结果分别如图9和表4所示。EDS结果表明，图9(a)、(b)中EDS 1和EDS 2区域的物相分别为θ-(Fe,Ni)(Al,Si)$_3$和τ_5-(Fe,Ni)$_{1.8}$Al$_{7.2}$Si。未加摆动时，断裂发生在IMCs层，焊缝侧断口观察到片状的τ_5-(Fe,Ni)$_{1.8}$Al$_{7.2}$Si，在钢侧断口观察到片状的θ-(Fe,Ni)(Al,Si)$_3$。τ_5-(Fe,Ni)$_{1.8}$Al$_{7.2}$Si相与θ-(Fe,Ni)(Al,Si)$_3$相之间的结合性能较差，与τ_5-(Fe,Ni)$_{1.8}$Al$_{7.2}$Si相相比，脆性的θ-(Fe,Ni)(Al,Si)$_3$相降低了接头的强度，在界面处形成的厚而脆的IMCs降低了接头的承载能力。铝/钢异种接头的界面层厚而脆，容易形成裂纹成为拉伸试验中的断裂源，导致接头在界面层发生断裂。基于上述原因，未加摆动时接头线载荷较低，属于脆性断裂模式。当摆动直径为2 mm、频率为30 Hz时，断裂发生在焊缝处，在此参数下接头IMCs的厚度均匀且仅由τ_5-(Fe,Ni)$_{1.8}$Al$_{7.2}$Si相组成，据Yang等[36]分析，与θ-(Fe,Ni)(Al,Si)$_3$/τ_5-(Fe,Ni)$_{1.8}$Al$_{7.2}$Si界面相比，单一τ_5-(Fe,Ni)$_{1.8}$Al$_{7.2}$Si/钢界面具有相对较低的晶面失配和更好的结合性能，从而提高了接头的力学性能。由表4所示的EDS 3结果可知，断口上存在α-Al和Al-Si共晶，且在断口上观察到许多韧窝，接头发生韧性断裂，如图9(c)所示。当摆动直径为4 mm时，接头断口主要是由Al-Si元素组成的凹坑，摆动直径增大导致激光中心能量密度降低，界面处的反应不充分导致结合性能差，接头强度降低，如图9(d)所示。

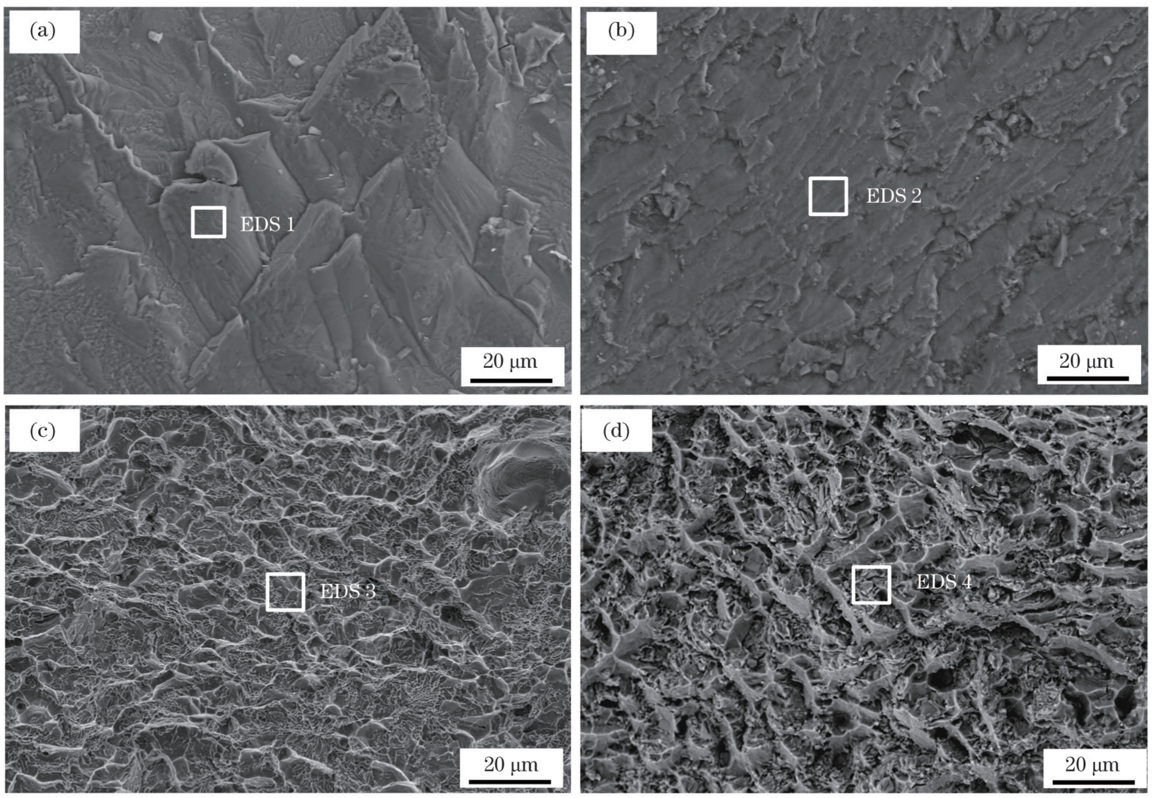

图9　不同摆动参数下铝/钢接头的断口形貌。(a)未加摆动时钢侧；(b)未加摆动时焊缝侧；(c)摆动频率30 Hz，摆动直径2 mm；(d)摆动频率30 Hz，摆动直径4 mm

Fig. 9　Fracture morphologies of Al/Fe joints under different welding parameters. (a) Fracture on steel side without rotation; (b) fracture on weld side without rotation; (c) rotating frequency of 30 Hz, and rotating diameter of 2 mm; (d) rotating frequency of 30 Hz, and rotating diameter of 4 mm

表4　图9所示区域的EDS结果

Table 4　EDS results of regions shown in Fig. 9

Region	Atomic fraction /%					Possible phase
	Al	Si	Fe	Ni	Cr	
EDS 1	66.61	8.34	17.35	1.35	5.99	θ-(Fe,Ni)(Al,Si)$_3$
EDS 2	70.41	10.01	13.18	0.75	5.65	τ_5-(Fe,Ni)$_{1.8}$Al$_{7.2}$Si
EDS 3	86.58	9.89	0.54	2.72	0.26	α-Al and Al-Si eutectic
EDS 4	89.37	8.90	0.73	1.0	0.01	α-Al and Al-Si eutectic

4 结 论

研究了摆动激光工艺参数对铝/镀镍钢激光熔钎焊接头组织和力学性能的影响。详细分析了铝/钢异种材料激光熔钎焊接头界面金属间化合物的形貌以及厚度，并对接头界面IMCs层的组成和力学性能进行了分析。得到以下结论：

1）与摆动频率相比，摆动直径对接头润湿宽度的影响较大。为了获得成形良好的摆动激光熔钎焊铝/钢接头，应在激光摆动直径为2 mm时优化焊接工艺参数。

2）激光未摆动时，在界面处形成了厚度约为8.45 μm的两层IMCs。激光摆动后，中间层厚度降低、种类减少。这是由于摆动激光降低了焊接峰值温度，抑制了脆性IMCs的形成。

3）当摆动直径为2 mm、频率为30 Hz时，接头线载荷达到了289.1 N/mm，比不摆动时提高了约33.9%，接头的断裂位置由未加摆动激光时的界面层断裂转变为焊缝断裂。

参 考 文 献

[1] Yang J, Oliveira J P, Li Y L, et al. Laser techniques for dissimilar joining of aluminum alloys to steels: a critical review[J]. Journal of Materials Processing Technology, 2022, 301: 117443.

[2] Li M F, Wang Y J, Yang S L, et al. Improving mechanical properties and electrode life for joining aluminum alloys with innovatively designated Newton ring electrode[J]. Journal of Manufacturing Processes, 2021, 64: 948-959.

[3] Tanaka T, Morishige T, Hirata T. Comprehensive analysis of joint strength for dissimilar friction stir welds of mild steel to aluminum alloys[J]. Scripta Materialia, 2009, 61(7): 756-759.

[4] El-Sayed M H, Naka M. Structure and properties of carbon steel-aluminium dissimilar joints[J]. Science and Technology of Welding and Joining, 2005, 10(1): 27-31.

[5] Sun J H, Huang J, Yan Q, et al. Fiber laser butt joining of aluminum to steel using welding-brazing method[J]. The International Journal of Advanced Manufacturing Technology, 2016, 85(9): 2639-2650.

[6] Yang J, Li Y L, Zhang H, et al. Dissimilar laser welding/brazing of 5754 aluminum alloy to DP 980 steel: mechanical properties and interfacial microstructure[J]. Metallurgical and Materials Transactions A, 2015, 46(11): 5149-5157.

[7] Torkamany M J, Tahamtan S, Sabbaghzadeh J. Dissimilar welding of carbon steel to 5754 aluminum alloy by Nd: YAG pulsed laser[J]. Materials & Design, 2010, 31(1): 458-465.

[8] Xia H B, Li L Q, Tan C W, et al. In situ SEM study on tensile fractured behavior of Al/steel laser welding-brazing interface[J]. Materials & Design, 2022, 224: 111320.

[9] Qiu R, Iwamoto C, Satonaka S. In situ scanning electron microscopy observation of fracture crack propagation in the welding interface between aluminium alloy and steel[J]. Materials Science and Technology, 2009, 25(10): 1189-1192.

[10] Xia H B, Tan C W, Li L Q, et al. In situ SEM observations of fracture behavior of laser welded-brazed Al/steel dissimilar joint[J]. Journal of Materials Engineering and Performance, 2018, 27(3): 1047-1057.

[11] 黄嘉森，蔡创，刘致杰，等. Inconel690镍基合金/SUS304不锈钢激光焊接接头组织与力学性能[J]. 光学学报，2023，43(10): 1014001.
Huang J S, Cai C, Liu Z J, et al. Microstructure and mechanical properties of laser welded Inconel690 nickel-based alloy/SUS304 stainless steel joints[J]. Acta Optica Sinica, 2023, 43(10): 1014001.

[12] 张佳琪，刘云祺，何绍雄，等. 超声振动钢/铝对接接头激光-MIG复合熔钎焊工艺研究[J]. 中国激光，2022，49(16): 1602013.
Zhang J Q, Liu Y Q, He S X, et al. Study on laser-MIG composite fusion brazing process of ultrasonic vibration steel/aluminum butt joint[J]. Chinese Journal of Lasers, 2022, 49(16): 1602013.

[13] Yu G Y, Wang H M, Chen S H, et al. Interfacial reaction between solid Ni and liquid Al in tens of seconds: dissolution kinetics of solid Ni and formation of intermetallic compounds[J]. Materials Characterization, 2020, 159: 110043.

[14] 崔佃忠，芦笙，崔晴晴，等. 焊接热输入对铝/镀锌钢CMT熔-钎焊接头组织与性能的影响[J]. 焊接学报，2014，35(9): 82-86，5.
Cui D Z, Lu S, Cui Q Q, et al. Effect of heat input on microstructure and mechanical properties of CMT welding-brazing joint between 5052 aluminum alloy and galvanized Q235 steel[J]. Transactions of the China Welding Institution, 2014, 35(9): 82-86, 5.

[15] Ozaki H, Kutsuna M, Nakagawa S, et al. Laser roll welding of dissimilar metal joint of zinc coated steel to aluminum alloy[J]. Journal of Laser Applications, 2010, 22(1): 1-6.

[16] 韩雨. 铝/钢异种材料摆动激光熔钎焊焊接特性研究[D]. 哈尔滨：哈尔滨工业大学，2020: 2-3，43-46.
Han Y. Study on welding characteristics of aluminum/steel dissimilar materials by swing laser fusion brazing[D]. Harbin: Harbin Institute of Technology, 2020: 2-3, 43-46.

[17] Xie J, Cai C, Zhang B B, et al. Microstructure evolution and fracture behavior of rotating laser welded-brazed 6061 aluminum alloys/304 SS dissimilar joint[J]. Materials Characterization, 2023, 195: 112543.

[18] Jiang Z G, Chen X, Li H, et al. Grain refinement and laser energy distribution during laser oscillating welding of Invar alloy[J]. Materials & Design, 2020, 186: 108195.

[19] 杨晖，李芳，华学明，等. 304L不锈钢扫描激光搭接焊熔池流动与焊缝成形研究[J]. 中国激光，2022，49(22): 2202004.
Yang H, Li F, Hua X M, et al. Study on weld pool flow and weld formation of 304L stainless steel by scanning laser lap welding[J]. Chinese Journal of Lasers, 2022, 49(22): 2202004.

[20] Chen S H, Li S Q, Li Y, et al. Butt welding-brazing of steel to aluminum by hybrid laser-CMT[J]. Journal of Materials Processing Technology, 2019, 272: 163-169.

[21] Xia H B, Tao W, Li L Q, et al. Effect of laser beam models on laser welding-brazing Al to steel[J]. Optics and Laser Technology, 2020, 122: 105845.

[22] Chen S H, Yu G Y, Li S Q, et al. Interfacial microstructures and mechanical property of Ni/Al dissimilar butt joint made by laser welding[J]. Journal of Manufacturing Processes, 2020, 50: 17-23.

[23] Tan C W, Zang C W, Zhao X Y, et al. Influence of Ni-coating thickness on laser lap welding-brazing of Mg/Ti[J]. Optics & Laser Technology, 2018, 108: 378-391.

[24] Chen S H, Yang D D, Zhang M X, et al. Interaction between the growth and dissolution of intermetallic compounds in the interfacial reaction between solid iron and liquid aluminum[J]. Metallurgical and Materials Transactions A, 2016, 47(10): 5088-5100.

[25] Rong J P, Kang Z F, Chen S H, et al. Growth kinetics and thickness prediction of interfacial intermetallic compounds between solid steel and molten aluminum based on thermophysical simulation in a few seconds[J]. Materials Characterization, 2017, 132: 413-421.

[26] Yang J, Chen J S, Zhao W Q, et al. Diode laser welding/brazing of aluminum alloy to steel using a nickel coating[J]. Applied Sciences, 2018, 8(6): 922.

[27] Jiang W M, Fan Z T, Li G Y, et al. Effects of zinc coating on interfacial microstructures and mechanical properties of aluminum/steel bimetallic composites[J]. Journal of Alloys and Compounds, 2016, 678: 249-257.
[28] Shi H J, Chai Y D, Li N, et al. Interfacial reaction mechanism of SiC joints joined by pure nickel foil[J]. Journal of the European Ceramic Society, 2020, 40(15): 5162-5171.
[29] Shi H J, Peng H B, Yan J Z, et al. Investigations of the effect of Si addition on graphite elimination and the oxidation behavior of SiC joint using Inconel 625 powder filler[J]. Journal of the European Ceramic Society, 2022, 42(4): 1258-1271.
[30] Li P, Yan Y, Lin J, et al. Interfacial bonding mechanism and joint weakness area of brazed SiC and Nb with AuNi filler alloy: first-principles and experimental perspective[J]. Journal of the American Ceramic Society, 2023, 106(10): 6255-6267.
[31] 董斌鑫, 张艳梅, 虞钢, 等. 304不锈钢/镍激光焊接中氧对接头形貌、组织及力学性能的影响[J]. 中国激光, 2022, 49(16): 1602004.
Dong B X, Zhang Y M, Yu G, et al. Effect of oxygen on morphology, microstructure and mechanical properties of 304 stainless steel/nickel laser welding joint[J]. Chinese Journal of Lasers, 2022, 49(16): 1602004.
[32] Yang J, Yu Z S, Li Y L, et al. Formation and toughening mechanisms of dispersions in interfacial intermetallics of dissimilar laser Al/steel joints[J]. Journal of Materials Engineering and Performance, 2018, 27(8): 4107-4114.
[33] Yu Y C, Huang W, Wang G Z, et al. Investigation of melting dynamics of filler wire during wire feed laser welding[J]. Journal of Mechanical Science and Technology, 2013, 27(4): 1097-1108.
[34] Wen Z L, Yu G Y, Li S Q, et al. Influence of Ni/Zn double coating on the steel on penetration welding-brazing by CMT arc-laser hybrid heat source[J]. Optics & Laser Technology, 2021, 134: 106602.
[35] Yu G Y, Zou T P, Chen S H, et al. Effect mechanism of Ni coating layer on the characteristics of Al/steel dissimilar metal brazing[J]. Materials Characterization, 2020, 167: 110518.
[36] Yang J, Hu A M, Li Y L, et al. Heat input, intermetallic compounds and mechanical properties of Al/steel cold metal transfer joints[J]. Journal of Materials Processing Technology, 2019, 272: 40-46.

Microstructure and Properties of Rotating Laser Welded-Brazed Aluminum/Nickel-Plated Steel Dissimilar Joint

Liu Yonghong, Cai Chuang*, Xie Jia, Zhang Bingbing, Yu Jie, Huang Jiasen

Key Laboratory of Advanced Technologies of Materials, Ministry of Education, School of Materials Science and Engineering, Southwest Jiaotong University, Chengdu 610031, *Sichuan, China*

Abstract

Objective The use of low-density lightweight materials, such as aluminum alloys, instead of traditional steel, titanium, and other materials to form a dissimilar material composite structure is an important way to achieve a light weight. Because of the different physical and chemical properties of aluminum alloys and steel, it is difficult to join aluminum and steel by laser welding-brazing. Brittle intermetallic compounds (IMCs) in the interface layer are easily produced owing to the small solid solubility between iron and aluminum. In this research, a rotating laser is applied to improve the temperature distribution and optimize the interface reaction. Based on the analysis of the morphology, type, and thickness of the interface layer of the aluminum/steel laser welding-brazing joint under different rotating parameters, the mechanical properties of the aluminum/steel welded joint are studied by a tensile test, and the fracture morphology and fracture mode of the joint are also investigated.

Methods The test materials are a 304 stainless-steel plate with a size of 100.0 mm×80.0 mm×0.9 mm and a 6061-T6 aluminum alloy sheet with a size of 100.0 mm×80.0 mm×1.2 mm. AlSi12 is used as filler wire. A fiber laser is used as the heat source. High-purity argon (volume fraction of 99.99%) with a gas flow rate of 25 L/min is used as the protective gas. After welding, the cross-sectional morphology of the weld is observed by using a metallographic microscope. A scanning electron microscope (SEM) is used to analyze the morphology and thickness of the IMC layer. The chemical composition of the interface layer is detected using an energy-dispersive X-ray spectroscope (EDS) system integrated with the SEM. The mechanical performance of the joint is represented by the line load. The fracture morphology is observed using the secondary electron detector of the SEM.

Results and Discussions After the addition of the rotating laser, the thickness of IMCs composed of θ-(Fe, Ni)(Al, Si)$_3$ and τ_5-(Fe, Ni)$_{1.8}$Al$_{7.2}$Si is significantly reduced, and the uniformity of the IMC layers is improved. The line load of the joint without a rotating laser is 215.9 N/mm. The joint with a rotation diameter of 2 mm has the largest line load of 289.1 N/mm, which is 33.9% higher than that without rotation. Compared with nonrotating-laser joints, the joint line load increases because of the thinning of the intermetallic layer and the reduction of the complexity of the IMC. At a rotation diameter of 2 mm and frequency of 30 Hz, a fracture occurs at the weld. Under these parameters, the IMC thickness of the joint is uniform and only composed of the τ_5-(Fe, Ni)$_{1.8}$Al$_{7.2}$Si phase. Compared with the θ-(Fe, Ni)(Al, Si)$_3$/τ_5-(Fe, Ni)$_{1.8}$Al$_{7.2}$Si interface, a single τ_5-(Fe, Ni)$_{1.8}$Al$_{7.2}$Si/steel interface achieves relatively low interface crystal plane mismatch and better bonding performance, thereby improving the tensile performance of the joint. In the EDS results in Table 4, α-Al and Al-Si eutectic on the fracture can be observed. Additionally, many dents are formed on the fracture, and the fracture mode is ductile fracture.

Conclusions Compared with the rotating frequency, the rotating diameter has a greater influence on the wetting width of the joint. To obtain a well-formed rotating laser welding-brazing aluminum/steel joint, the welding process parameters should be optimized with a laser rotating diameter of 2 mm. When the laser is not rotating, two layers of IMCs with a thickness of approximately 8.45 μm are formed at the interface. After the rotating laser is applied, the thickness of the intermediate layer is reduced, and the variety is decreased. The rotating laser reduces the welding peak temperature and inhibits the formation of brittle IMCs. At a laser rotation diameter of 2 mm and frequency of 30 Hz, the linear load reaches a maximum value of 289.1 N/mm, which is approximately 33.9% higher than that without the rotating laser. The fracture position of the joint changes from the interface layer without the rotating laser to the weld.

Key words laser technique; Al/steel laser welding-brazing; rotating laser; intermetallic compound; mechanical property